ACS NANO

www.acsnano.org

ARTICLE

Quantification of mRNA Expression Using Single-Molecule Nanopore Sensing

Yana Rozevsky, Tal Gilboa, Xander F. van Kooten, Dennis Kobelt, Diana Huttner, Ulrike Stein,* and Amit Meller*

Cite This: *ACS Nano* 2020, 14, 13964–13974

Read Online

ACCESS | Metrics & More | Article Recommendations | Supporting Information

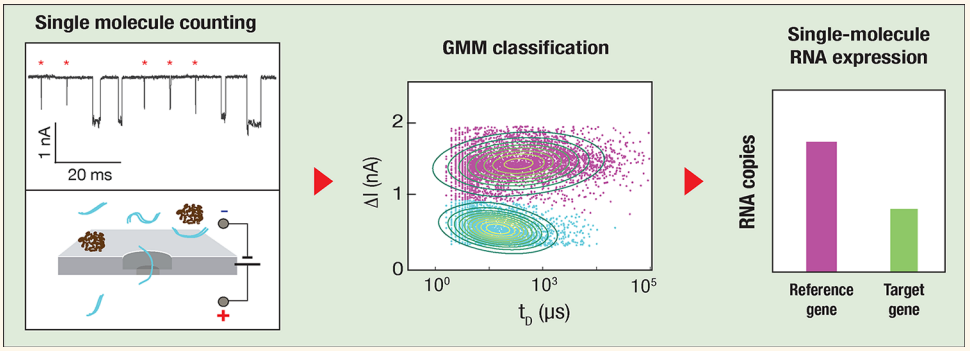

ABSTRACT: RNA quantification methods are broadly used in life science research and in clinical diagnostics. Currently, real-time reverse transcription polymerase chain reaction (RT-qPCR) is the most common analytical tool for RNA quantification. However, in cases of rare transcripts or inhibiting contaminants in the sample, an extensive amplification could bias the copy number estimation, leading to quantification errors and false diagnosis. Single-molecule techniques may bypass amplification but commonly rely on fluorescence detection and probe hybridization, which introduces noise and limits multiplexing. Here, we introduce reverse transcription quantitative nanopore sensing (RT-qNP), an RNA quantification method that involves synthesis and single-molecule detection of gene-specific cDNAs without the need for purification or amplification. RT-qNP allows us to accurately quantify the relative expression of metastasis-associated genes MACC1 and S100A4 in nonmetastasizing and metastasizing human cell lines, even at levels for which RT-qPCR quantification produces uncertain results. We further demonstrate the versatility of the method by adapting it to quantify severe acute respiratory syndrome coronavirus 2 (SARS-CoV-2) RNA against a human reference gene. This internal reference circumvents the need for producing a calibration curve for each measurement, an imminent requirement in RT-qPCR experiments. In summary, we describe a general method to process complicated biological samples with minimal losses, adequate for direct nanopore sensing. Thus, harnessing the sensitivity of label-free single-molecule counting, RT-qNP can potentially detect minute expression levels of RNA biomarkers or viral infection in the early stages of disease and provide accurate amplification-free quantification.

KEYWORDS: *nanopore, single-molecule counting, mRNA expression, SARS-CoV-2, MACC1, S100A4*

Molecular methods for quantitative gene expression down to the single-cell level have enabled analysis of diverse biological pathways and are therefore regarded as key tools in the life sciences. Particularly, single-molecule (SM) techniques, such as SM fluorescence *in situ* hybridization (smFISH) and single-molecule arrays, have allowed quantification of low-abundance targets by relying on molecular counting rather than ensemble measurements.[1] However, most SM RNA quantification methods are based on fluorescence imaging of immobilized molecules, which significantly increases their complexity and requires elaborate laboratory equipment. By contrast, nanopores are relatively simple analytical sensors that enable label-free counting of individual nucleic acid molecules in solution using low-cost and

Received: July 30, 2020
Accepted: September 15, 2020
Published: September 15, 2020

https://dx.doi.org/10.1021/acsnano.0c06375
ACS Nano 2020, 14, 13964–13974

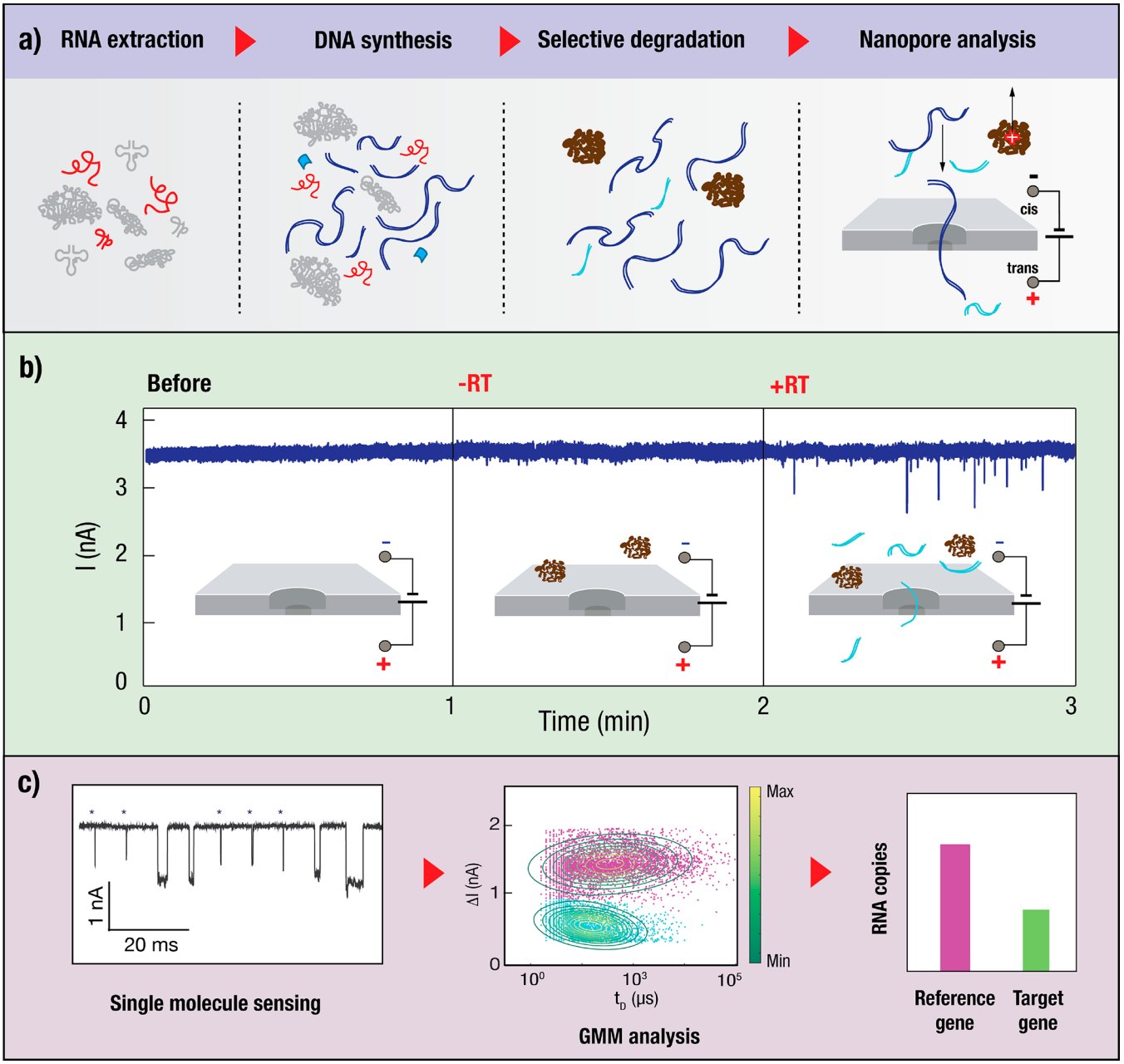

Figure 1. Single-molecule mRNA expression analysis using nanopores. (a) Three consecutive biochemical steps prepare mRNA (or RNA) molecules for nanopore analysis. (i) RNA is extracted from cells or clinical samples. (ii) Transcripts of interest are converted to cDNAs of specific lengths by reverse transcription followed by second strand DNA synthesis and optional amplification. (iii) The sample is subjected to digestion using RNase 1 and ProK to remove off-target molecules (and optional ExoI digestion to produce cDNA blunt ends). (b) Experimental validation of the RNA sensing method: 50 ng of DNaseI-treated total RNA, extracted from SW620 cells, was subjected to reverse transcription in the presence of the RT enzyme (+RT) or without it (−RT), using gene-specific primers. Panels (left to right) show the nanopore ion current trace before addition of the analytes, addition of −RT sample, and addition of the +RT sample. (c) Each DNA translocation event is analyzed to extract its electrical characteristics. A Gaussian mixture model (GMM) is used to cluster events and to classify the molecules to quantify the expression of the target gene relative to a reference.

portable equipment, while potentially offering high sensitivity and high throughput.[2,3]

A solid-state nanopore (ssNP) sensor is a nanometer-scale pore fabricated in a freestanding insulating membrane separating two electrolytic solutions.[4,5] In the presence of an electric field, electrically charged analytes are threaded through the nanopore, resulting in a distinct reduction in the ionic current with an amplitude and duration corresponding to the cross section and length of the translocating molecule.[6] The ability of ssNPs to resolve single-molecule stems from their nanometric dimensions, which are on par with the analytes' cross section. In the past decade, NP sensing has been demonstrated for a variety of biomolecules, including multiple DNA forms,[7−9] RNA,[10,11] and proteins.[12−15] Moreover, several biochemical assays have been proposed in order to overcome the resolution limits of ssNP sensing by treatment of the sample to include biochemical modifications[9,16−19] or by using restriction enzymes.[20] To date, however, ssNP-based quantification of

https://dx.doi.org/10.1021/acsnano.0c06375
ACS Nano 2020, 14, 13964−13974

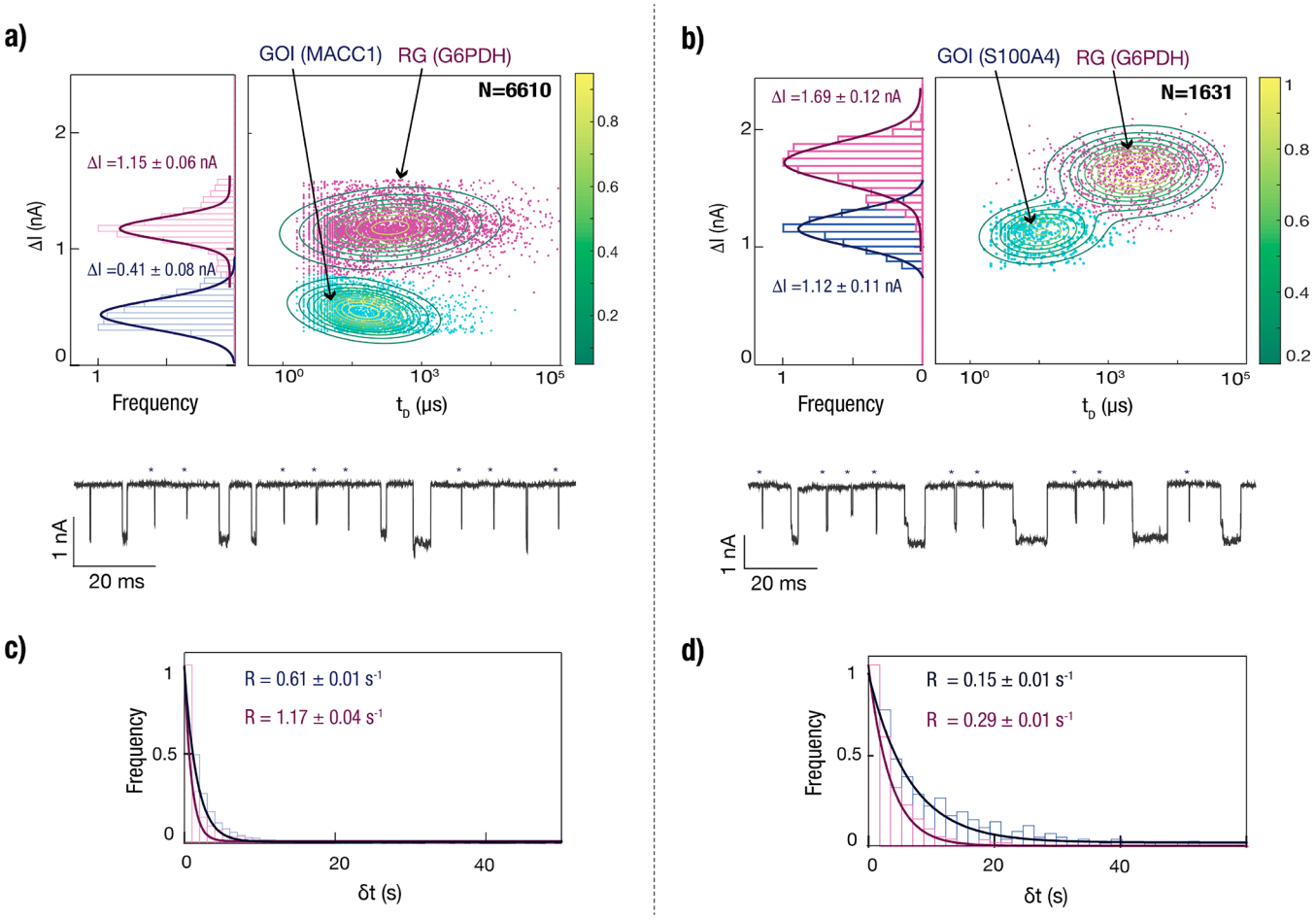

Figure 2. Validation of GMM classification of multiple genes by RT-qNP. Top panel: scatter plots and the associated histograms obtained (a) for a mixture of 0.5 nM MACC1 (360 bp) and 1 nM G6PDH (1231 bp) cDNAs and (b) for a mixture of 0.5 nM S100A4 (123 bp) and 1 nM G6PDH cDNAs. The conductance of the pores was 15.2 and 22.7 nS, respectively. The translocation events of each sample mixture were classified using a two-dimensional GMM algorithm. The fitted Gaussian mixture contours are overlaid on the scatter plots. We attribute the populations with shorter t_D and lower ΔI (blue) to the gene of interest (GOI) and the populations having the longer t_D and higher ΔI (purple) to the reference gene (RG). Representative concatenated events for each sample mixture are shown. Shorter events representing the GOI are marked with asterisks. Bottom panels: distribution of the capture rate for (c) MACC1 and (d) S100A4. Results for the GOI and the RG are plotted in blue and purple, respectively. The capture rates were approximated by exponential fit to the histograms resulting in the following values: (c) 0.61 ± 0.01 and 1.17 ± 0.05 s^{-1} for MACC1 and G6PDH, respectively, and (d) 0.15 ± 0.01 s^{-1} and 0.29 ± 0.01 s^{-1} for S100A4 and G6PDH, respectively.

endogenous RNA copy number has only been possible after extensive purification steps, which lead to loss of valuable analyte and may prohibit sensing at low RNA expression levels. Nanopore detection of unpurified biological samples is highly challenging due to the large number of background species that produce complex signals and may block the pore.

Molecular amplification methods have been found to bypass these issues. Specifically, reverse transcription quantitative real-time polymerase chain reaction (RT-qPCR) is the method of choice for RNA quantification, often serving as a reference method.[21] However, despite the widespread use of RT-qPCR for RNA quantification, its accuracy at low target copy numbers is insufficient, as the extensive amplification that is required to produce a detectable signal may introduce errors such as off-target amplification and amplification biases.[22]

Here, we introduce RT-qNP, a ssNP-based sensing method for SM quantification of low-abundance RNA molecules in biological samples. The method consists of a series of enzymatic reactions that convert target RNA into double-stranded complementary DNA (ds-cDNA) of defined lengths and digest off-target molecules and unwanted species without the need for lossy purification steps. The synthesized cDNA molecules are digitally counted by a ssNP device, allowing multiplexed quantification of several genes. Although the cDNA can be detected without any amplification, an optional low-level amplification step (1−4 cycles) leads to an increase in the detection rate. Importantly, our method increases the detection confidence and reduces the assay time, while preserving the original gene expression levels. Finally, RT-qNP is compatible with sample volumes of just a few microliters, potentially broadening its clinical utility.

We demonstrate our method in the context of two diverse and significant biological systems. First, we show that RT-qNP can be used to count the relative mRNA overexpression in genes associated with tumor metastasis. Importantly, our method reliably quantifies relative changes in expression between nonmetastasizing and metastasizing cell lines, in agreement with the RT-qPCR results. A direct comparison between the RT-qNP method and RT-qPCR shows that our method can sense >5 orders of magnitude fewer copies of cDNA.

https://dx.doi.org/10.1021/acsnano.0c06375
ACS Nano 2020, 14, 13964−13974

Consequently, the MACC1 biomarker, which cannot be detected with confidence by RT-qPCR in the nonmetastasis cell line, is accurately quantified by RT-qNP. Finally, we adapted our method for quantification of SARS-CoV-2 RNA, with the human "housekeeping" gene RPP30 serving as a reference. By eliminating the need for PCR amplification, we believe RT-qNP can substantially reduce diagnostic errors in clinical samples with low abundance of SARS-CoV-2 RNA, while offering a versatile alternative to the RT-qPCR platforms.

RESULTS AND DISCUSSION

Single-Molecule mRNA Quantification Using Solid-State Nanopore Biosensors. In RT-qNP, total RNA is extracted from either cells or any other biological source, and all subsequent steps are additive and do not entail any purification steps (Figure 1). First, cDNA is synthesized by RT, followed by synthesis of the second DNA strand by a DNA polymerase. Next, RNase 1 and Proteinase K (ProK) are added in subsequent steps to digest all remaining RNA and proteins. Finally, the product is introduced directly to the nanopore for label-free analysis. Translocation of the negatively charged double-stranded cDNA through the NP leads to a distinct drop in the ionic current, whereas the remaining undigested enzymes are electrophoretically repelled from the NP, and digested RNA or enzymes cause only brief current blockages that are easily filtered in the signal processing stage.

Figure 1b shows an experimental validation of the conversion process, in which we processed two samples from the same RNA source either with or without reverse transcriptase (termed "+RT" and "−RT", respectively). Each sample contained 50 ng of total RNA and gene-specific primers to produce a 360 bp amplicon in the MACC1 open reading frame (see Methods and SI Figure S1). The open-pore ionic current was stable before the sample was added. At $t = 1$ min, the −RT sample was introduced to the *cis* side of the NP, resulting in a mild increase in the electrical noise, presumably due to the free digested nucleotides in the solution; however, no ionic current events are observed. At $t = 2$ min, the +RT sample was added, leading to clear translocation events (Figure 1b, right panel). In a separate experiment, we continuously recorded the open-pore current for an extended period of 10 min after the addition of the −RT sample, confirming that no nonspecific translocation events occur unless cDNA is synthesized by the reverse transcriptase (SI Figure S2). Another control experiment, in which ~10^3-fold more concentrated +RT product was purified using a commercial cleanup kit, showed nearly identical statistical distributions to the ones recorded using our purification-free method (SI Figure S3), indicating that the observed translocation events in the unpurified sample were specifically caused by the cDNA product.

The final step of the NP sensing method is shown in Figure 1c. First, we collected and analyzed translocation events based on their blockage current amplitude (ΔI) and dwell time (t_D). We then applied a peak-finding algorithm to 2D density plots of ΔI *versus* $\log(t_D)$ to obtain the initial conditions for a statistical analysis using a Gaussian mixture model (GMM) algorithm.[20] The GMM efficiently resolves populations of events in a mixture containing two or three types of DNA. Between 100 and 1000 events are typically sufficient to produce statistically robust data sets. The relative quantities of double-stranded cDNA reverse transcribed from different genes can then be calculated either from the total number of events in each cluster or from the relative event rates of the populations.

Nanopore Quantification of Mixtures Containing Multiple cDNAs. To characterize the ability of our method to quantify relative concentrations of cDNAs in a mixture, we performed nanopore measurements using a mixture of two cDNAs, each containing a gene of interest (GOI) and a reference gene (RG). In these experiments, the cDNA was sufficiently amplified and purified using standard procedures to allow accurate quantification of the cDNA concentrations using UV−Vis spectrometry. The GOI was either MACC1 (360 bp) or S100A4 (123 bp), and the RG was G6PDH (1231 bp) (see Methods).

Figure 2a shows the event density plot and concatenated ionic current traces obtained from a mixture of 0.5 nM MACC1 and 1 nM G6PDH. The two populations of translocation events are clearly separated in both ΔI and t_D. A GMM analysis of the data identifies two populations (see Methods), from which we calculate the two populations' arrival time histograms (Figure 2c). Exponential fits of the histograms yielded event rates of 0.61 ± 0.01 and 1.17 ± 0.04 s^{-1} for MACC1 and G6PDH, respectively. The ratio of these two event rates is 0.52 ± 0.03, which closely matches the ratio of concentrations in the mixture. Additional nanopore results from a mixture of 0.5 nM S100A4 and 1 nM G6PDH are shown in Figure 2b, yielding two distinct populations and arrival time histograms with event rates of 0.15 ± 0.01 s^{-1} for S100A4 and 0.29 ± 0.01 s^{-1} for G6PDH, a factor of 0.52 ± 0.04 (Figure 2d). The ratio of event rates determined by the GMM closely matches the concentration ratio of the two cDNA species in the mixture, highlighting the robustness of the method. The event classification is accurate despite slight differences in the DNA lengths and nanopore diameter between experiments, both affecting the absolute event rate measurements. We therefore conclude that, after GMM classification based on arrival time, histograms can provide a robust estimation for relative cDNA concentration, and that relative quantification against an internal reference gene can compensate for variability between pores and experiments.

RT-qNP Analysis of mRNA Expression in Nonmetastatic and Metastatic Isogenic Cell Lines. mRNA expression levels of MACC1 and S100A4 genes have been independently shown to affect cancer pathways that are altered before and during the onset of the metastatic phase.[23,24] From a clinical standpoint, the expression levels of MACC1 and S100A4 have been shown to be prognostic and predictive indicators for metastatic onset in various cancers.[23,25−38] Moreover, additive overexpression of the two genes strongly correlates with tumor aggressiveness.[27,30,32] Therefore, an accurate quantification of the expression levels of these two genes may provide insight into the molecular events leading to the onset of metastasis.

We used RT-qNP analysis to determine the mRNA expression levels of MACC1 and S100A4 relative to the reference gene G6PDH in nonmetastasizing and metastasizing isogenic colorectal cancer (CRC) cell lines. SW480 cells were isolated from a primary adenocarcinoma in the colon, whereas SW620 cells were derived from a lymph node of the same individual after cancer recurrence with widespread metastasis.[25] In four separate experiments, we evaluated relative populations' event rates of 16-fold amplified cDNA. Validation of multiplexed sample preparation from each cell line by gel analysis is shown in SI Figure S5. Our results are summarized in Table 1. Raw translocation events are shown in Figure 3, as well as the density diagrams which were used as initial predictors for GMM-based analysis. The top two panels correspond to the MACC1 analysis and the bottom panels to S100A4, as indicated. In all cases, the

https://dx.doi.org/10.1021/acsnano.0c06375
ACS Nano 2020, 14, 13964−13974

Table 1. Summary of the Nanopore Results of Multiplexed Mixture Samples Prepared in SI Figure S5 and Assayed in Figure 3[a]

sample		ΔI (nA)	t_D (μs)	R (s^{-1})
SW480	MACC1	1.17 ± 0.27	31.0 ± 0.4	1.86 ± 0.13
	G6PDH	1.48 ± 0.23	182.0 ± 12.3	1.79 ± 0.08
SW620	MACC1	0.68 ± 0.16	50.7 ± 0.6	5.81 ± 0.06
	G6PDH	0.92 ± 0.10	365.0 ± 13.0	1.89 ± 0.03
SW480	S100A4	0.58 ± 0.06	60.3 ± 1.6	0.78 ± 0.05
	G6PDH	1.50 ± 0.21	76.5 ± 4.1	1.75 ± 0.04
SW620	S100A4	1.33 ± 0.25	27.0 ± 0.5	0.88 ± 0.06
	G6PDH	2.05 ± 0.15	505.0 ± 73.0	1.58 ± 0.08

[a] ΔI denotes the event amplitude, t_D is the dwell time, and R is the events' arrival rate.

corresponding event arrival time histograms were generated and fitted by exponential functions, and GMM-based event classification was applied.

The mean event rates for the RG, calculated from the arrival time histograms in each data set, are shown in Figure 4a in dark green. We consistently obtained similar absolute rates (roughly 1.75 events/s) in all experiments with small differences attributed primarily to pore-to-pore variations. This indicates that G6PDH expression can be used for reliable normalization in both cell lines. The relative capture rates, shown in light green, indicate a ∼3-fold higher MACC1 mRNA content in the metastasizing cell line compared to the nonmetastasizing one. In contrast, we found only a minor difference in S100A4 expression between the two, and the expression of this gene was lower than that of the RG.

We compared the results from the RT-qNP method to an RT-qPCR benchmark.[39,40] To quantify gene expression using RT-qPCR, we constructed a calibration curve of the threshold cycle (C_t) for known concentrations of RNA (see SI Figure S6) and used it to determine the concentration of GOI and RG mRNA in CRC samples. The relative expression (RE) of each gene was calculated as the ratio between the GOI and RG concentrations, both normalized to the concentration of that gene in the metastasizing cell line, SW620 (see Methods). To directly compare the results, we normalized RT-qNP measurements in the same way, with event population rates substituted for concentrations.

The results in Figure 4b show good agreement between the RT-qPCR and RT-qNP results, indicating that the relative event rates accurately reflect mRNA abundance in the sample. Strikingly, however, the MACC1 expression in the non-metastasizing SW480 cell line was too low to be detected using RT-qPCR. By contrast, RT-qNP sensing identified a small yet resolvable quantity of MACC1 (Figure 4b, left green bar, and repeats in SI Figure S12). This result highlights the sensitivity of nanopore sensing for quantification of MACC1 mRNA at low concentrations, while maintaining specificity in the classification of translocation events based on their amplitude and dwell time.

RT-qNP mRNA Quantification Compared with RT-qPCR. To determine how ssNP sensing at low initial RNA concentrations can benefit from limited amplification, we modified the assay to include cDNA amplification starting from 16-fold (4 cycles) down to 2-fold (1 cycle). Figure 5a shows the results of RT-qNP sensing of MACC1 cDNA reverse transcribed from 50 ng of total RNA extracted from SW620 cells. Typical continuous 3 min ionic current traces are shown in the top panel of Figure 5a. Notably, even in the extreme case of 2-fold amplification, tens of events were collected in ∼20 min, and the GMM algorithm identified a single population with similar properties in each of the three cases, indicating that the events are indeed related to MACC1 cDNA. The extreme sensitivity of the RT-qNP sensing is clearly attributed to our sample generation process, as the inclusion of any purification steps would render the ssNP measurements impractical, requiring at least ∼1000-fold amplification.

Figure 5b shows a direct comparison of the sensitivity of RT-qNP sensing and RT-qPCR for detecting MACC1, in terms of capture rate (for the NP) or fluorescence intensity (for RT-qPCR). The capture rate of the ssNP follows the expected exponential increase from 1 to 7 amplification cycles and eventually saturates at high concentrations of cDNA as the mean interevent time approaches the translocation dwell time. In all cases, we evaluated the average event capture rate from a few tens of events to >2000 events. Errors were established from exponential fits to the event capture rate histograms (SI Figure S7). RT-qPCR amplification using the same 50 ng of total RNA sample and primer set required ∼20 amplification cycles before a detectable signal was produced.[41,42] The RT-qPCR analysis shown here represents optimized PCR primer set sensing (see SI Figure S8 and the primers sequences in SI Table S3), indicating that the RT-qNP method provides a ∼250,000-fold sensitivity improvement, as compared to RT-qPCR.

RT-qNP Analysis of SARS-CoV-2 RNA. The COVID-19 pandemic has highlighted the importance of RNA detection as a diagnostic tool. Currently, the vast majority of nucleic acid tests are based on RT-qPCR amplification of a SARS-CoV-2 gene, such as RdRp or ORF-1b.[43−45] These tests are not quantitative, and their binary diagnostic outcome is based on an empirical threshold of amplification cycles (commonly 35 or 40) rather than on quantitative RNA abundance. The arbitrary nature of the diagnostic threshold and its variability among tests that use different primers complicates comparisons of viral load and may lead to false diagnosis.[46] Quantification of viral RNA against a reference gene may provide a way to overcome these challenges.

To illustrate the versatility of RT-qNP, we adapted the method to quantify SARS-CoV-2 viral RNA against a human reference gene (RPP30) of known concentration. Although the workflow remained conceptually identical to the one shown in Figure 1, we combined the RT and double-stranded cDNA synthesis in a single reaction, using WarmStart RTx (NEB) and Bst 2.0 (NEB) to shorten the reaction time and further improve its overall efficiency (see SI-1). To increase the detection sensitivity, we used two sets of primers targeting the viral RNA and one targeting the human RPP30 gene (see Methods and SI Table S3). No downstream PCR amplification was required for the nanopore measurements.

Figure 6a−c shows nanopore results of cDNA detection after conversion from SARS-CoV-2 RNA (2500 copies) and total human mRNA (0.25 ng) from HCT116 cell lines. The primers for the viral and human sequences, respectively, yielded cDNA fragments 107−108 and 758 bp in length (see SI Figure S9). The GMM analysis successfully distinguished two populations of translocation events (Figure 6b), and an exponential fit to the event arrival time (Figure 6c) yielded relative event rates for the two targets.

We performed RT-qNP quantification over a clinically relevant concentration range of synthetic SARS-CoV-2 RNA (1250−5000 copies), mixed with RPP30 mRNA extracted from a fixed amount of 0.25 ng total human RNA from HCT116 colon cancer cell line. Figure 6d shows the event rate of CoV-2

https://dx.doi.org/10.1021/acsnano.0c06375
ACS Nano 2020, 14, 13964−13974

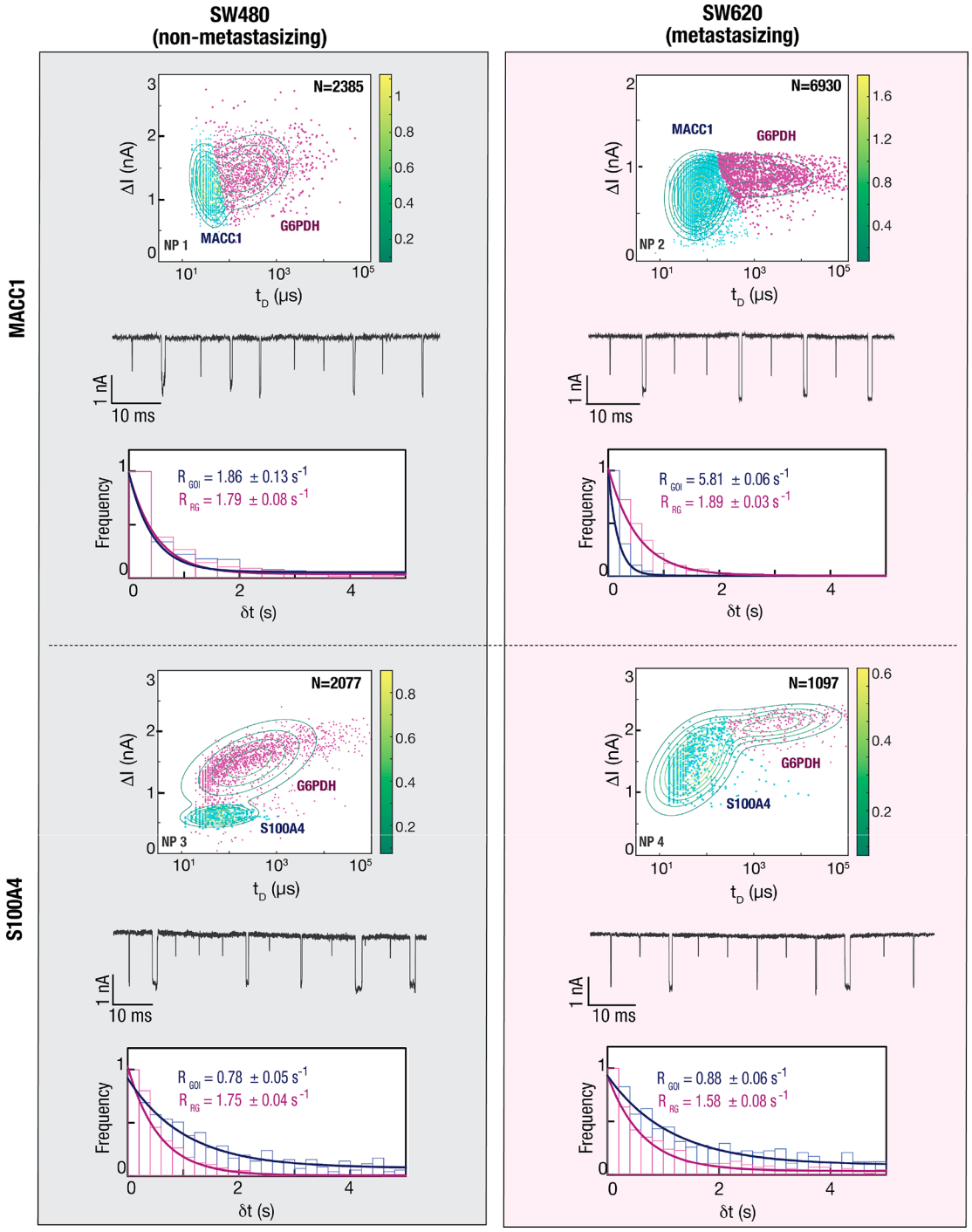

Figure 3. NP quantification of mRNA expression levels in isogenic nonmetastasizing and metastasizing cell lines. MACC1, S100A4, and reference gene G6PDH cDNAs originated from nonmetastatic and metastatic cell lines (SW480 and SW620, respectively), processed by RT-qNP and subjected to 16-fold amplification. Event scatter plots, representative translocation events, histograms of the dwell times, and the current blockages are shown for each of the four experiments. GMM analysis was applied to classify the events into two populations representing RG and the GOI, as indicated. Gaussian mixture contours are overlaid on top of the scatter plots. All experiments were conducted using pores with average conductance of 10.5 ± 2 nS.

relative to the comeasured RPP30 as a function of the number of RNA copies used in the upstream conversion process. Event diagrams and histograms for each of the concentrations are shown in SI Figure S10. The outstanding linearity of the relative event rate across multiple pores and independently prepared samples suggests that RT-qNP can be used to quantify small changes in relative abundance. Combined with the fact that no PCR amplification is required, this result underlines the potential of single-molecule RNA detection methods for accurate quantification of viral load.

CONCLUSIONS

RT-qNP enables quantification of RNA levels *via* reverse transcription and subsequent single-molecule counting of double-stranded cDNA molecules. This method offers several advantages over other common RNA quantification techniques,

https://dx.doi.org/10.1021/acsnano.0c06375
ACS Nano 2020, 14, 13964−13974

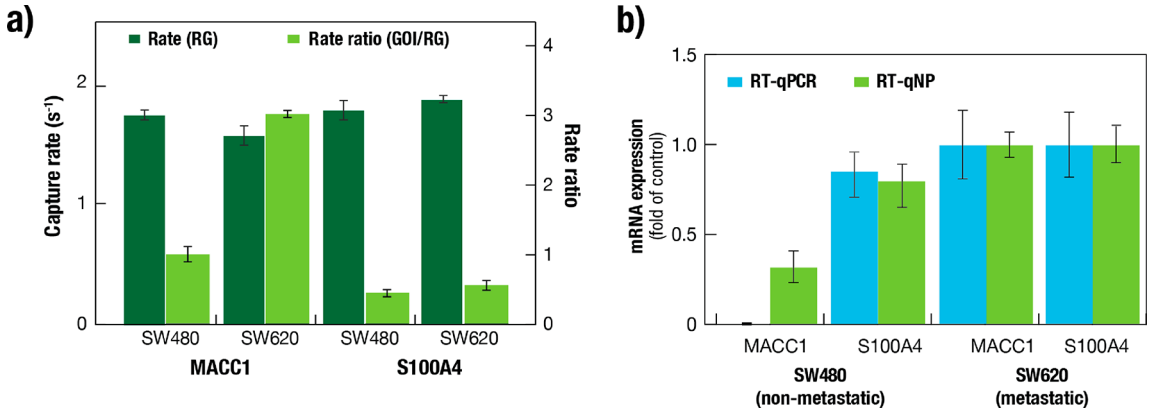

Figure 4. Comparison between RT-qNP and RT-qPCR quantification of mRNA expression levels in isogenic nonmetastasizing and metastasizing cell lines. (a) Absolute translocation event rate of G6PDH (left axis, dark green bars) and the event rate relative to the GOI (right axis, light green bars) measured for the four samples in Table 1. All experiments resulted in similar event rates for the RG with an average of 1.75 ± 0.03 s^{-1}. The relative event rate of the GOI to RG is increased from the nonmetastatic to the metastatic cell lines, where the most substantial increase is detected for MACC1: 0.5 and 1.7 s^{-1} for nonmetastasizing and metastasizing samples, respectively. (b) Comparison of the relative mRNA quantification results obtained using RT-qNP (green bars) or RT-qPCR (blue bars). The expression levels in each of the four samples were normalized to the results of the metastatic cell line (SW620). PCR error bars represent the standard deviation for duplicate reactions calculated using error propagation.

such as RT-qPCR. First, by avoiding nonlinear amplification, our method preserves the linear relation between the number of detected cDNA molecules and the number of RNA copies in the sample. PCR can suffer from bias and off-target amplification, which may hinder the accurate quantification of RNA transcripts at low copy number. Second, bypassing nucleic acid amplification greatly simplifies the upstream sample treatment in RT-qNP. The compatibility with small sample volumes, short process time, and lack of thermal cycling are crucial factors for future implementations of single-molecule biosensors in mobile and miniature devices.

The ability to estimate the length of each detected molecule substantially improves the signal-to-background ratio and ensures correct detection without the need for specific labeling. We used this feature to identify cDNA from multiple genes in the same sample, enabling quantification of expression levels relative to a reference gene, acting as an internal control. Although we demonstrated simultaneous detection of two genes in a mixture, we expect that the multiplexity can be vastly extended by further developments in the field of nanotechnology. For instance, 2D materials offer superior measurement bandwidth and low noise, which could further boost the dynamic range of our method by several orders of magnitude.[47−50] The addition of simultaneous optical sensing alongside electrical measurements could further extend the multiplexity of this method,[51] whereas the use of preconcentration techniques such as isotachophoresis can enhance the event rate if limited amplification is not possible.[52]

Currently, the relative expression levels of key mRNA biomarkers, such as MACC1 and S100A4, are used for cancer metastasis prognosis. Nevertheless, basic and clinical research in this area would benefit significantly from the analysis of submilliliter plasma samples derived from model animals, which remains challenging for RT-qPCR due to low abundance of cell-free mRNAs in the plasma. The ability to routinely quantify these genes and other emerging mRNAs in clinical samples with single-molecule precision may therefore facilitate development of early cancer diagnostics.

The RT-qNP RNA quantification method presented is versatile and can be directly applied in many fields of biological and medical research. As an example, we adapted our method to address the acute need for high-resolution sensing of the novel SARS-CoV-2 RNA, showing that it can be readily quantified simultaneously with the human RPP30 gene used as a reference and a quality control factor of the samples. Single-molecule counting of the two RNA types produces a linear relationship between the measured event rate and SARS-CoV-2 RNA copy number in a range that is often encountered in clinical testing. In this case, PCR amplification was eliminated entirely, allowing direct counting of cDNA molecules. On top of the improved accuracy, the elimination of PCR amplification highly simplifies the overall biochemical assay, potentially reducing the sample test time and reagents cost. Future and ongoing work will investigate the accuracy of RT-qNP using clinical samples, directly comparing it to the diagnostic RT-qPCR results.

To summarize, we presented here an RNA quantification method which holds two important advantages. First, purification-free processing of complex biological samples, which we tailored to the requirements of the ssNP sensor permits applications of label-free RNA sensing in biological research. Second, amplification-free sensing provides accurate quantification of transcript copy number and circumvents potential biases and disadvantages arising from enzymatic amplification methods.

METHODS

Sample Preparation for Nanopore Experiments. Either DNaseI-treated RNA extracted from human cells or SARS-CoV-2 RNA (control 2, MN908947.3, Twist 102024.1) was reverse transcribed with specific primers (SI Table S1 or Table S3) and either subjected to second strand synthesis or to PCR amplification (see sample preparation scheme in Figure 1). Prior to nanopore sensing experiments, the samples were either subjected to serial enzymatic digestion steps ("purification-free" sample) or purified using a commercial PCR cleanup kit. See detailed information on enzymes used and the reaction conditions for each sample type in SI Notes 1.

Cell Lines. Human CRC cell lines (SW480, SW620, RKO, and HCT116) were purchased from American Type Culture Collection (ATCC; Manassas, VA). The cells were cultured either in RPMI (SW480) or in DMEM (SW620) media supplemented with 10% fetal calf serum. These adherent cell lines were grown in flasks in a

https://dx.doi.org/10.1021/acsnano.0c06375
ACS Nano 2020, 14, 13964−13974

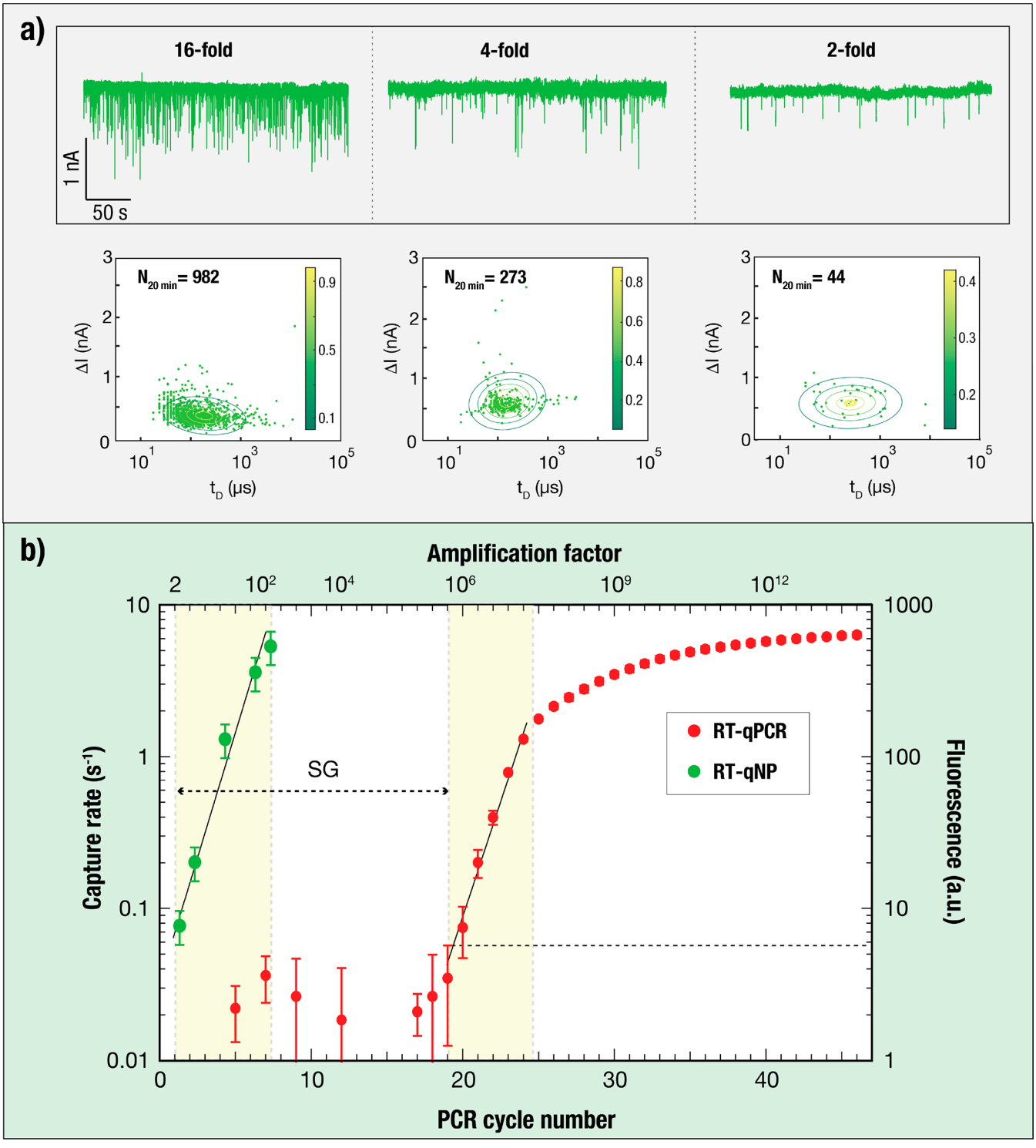

Figure 5. Evaluation of the sensitivity of RT-qNP for mRNA quantification. (a) Top: raw continuous ion current recordings of MACC1 cDNA prepared using RT-qNP, subjected to 16-, 4-, and 2-fold amplification and measured using 4.5 nm pores. Bottom: event diagram showing similar event amplitudes and dwell times for the three experiments, analyzed using the GMM. Green dots represent the total number of events detected in the first 20 min of each experiment. (b) Comparison of MACC1 gene expression analysis using RT-qPCR (right axis, red) and RT-qNP (left axis, green), starting from the same source of 50 ng of total RNA extracted from SW620 cells. The total fluorescence (for RT-qPCR) and the capture rate (for RT-qNP) are plotted as a function of the number of PCR cycles. The exponential regime for each method is indicated by yellow boxes. Measurements were performed in triplicate. Error bars represent the standard deviations of measurements. The C_t value of the RT-qPCR is estimated as 20 cycles. SG indicates the sensitivity gap.

humidified incubator at 37 °C with 5% CO_2 and harvested at 80% confluency for subsequent total mRNA extraction. All used cell lines were authenticated by genotyping and were confirmed to be mycoplasma-free.

https://dx.doi.org/10.1021/acsnano.0c06375
ACS Nano 2020, 14, 13964−13974

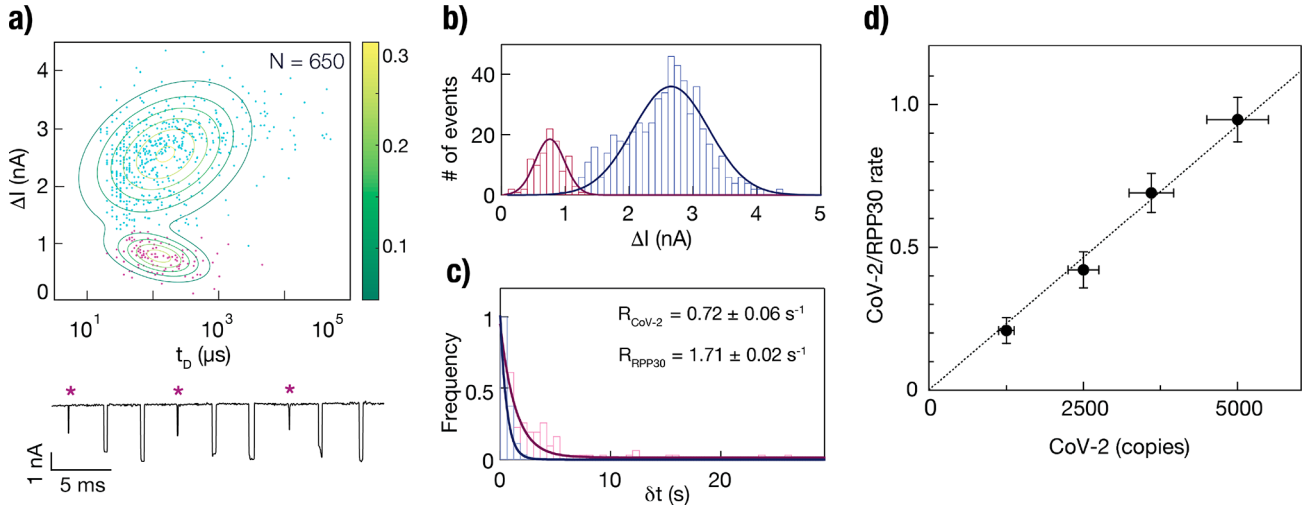

Figure 6. RT-qNP quantification of SARS-CoV-2 RNA against the human reference gene RPP30. (a) Top: event diagram showing nanopore translocations of cDNA synthesized from 2500 copies SARS-CoV-2 RNA and RPP30 from 0.25 ng of total RNA from HCT116 cells. Two populations were clearly distinguished by the GMM. Bottom: concatenated ionic current traces showing representative translocation events. Short and shallow events, associated with SARS-CoV-2 cDNA, are marked with an asterisk. Histograms of the current blockage (b) and event arrival time (c) show two populations with distinct event rates. (d) Relative event rate of SARS-CoV-2 and RPP30 detection as a function of the starting copy number of SARS-CoV-2 RNA. The amount of RPP30 was kept constant at 0.25 ng of total RNA.

Device and Nanopore Fabrication. Nanopore chips were fabricated on a 4 in. silicon wafer coated with silicon dioxide (SiO_2, 500 nm) and low-stress amorphous silicon nitride (SiN_x, 50 nm). The SiN_x was locally thinned to 8−10 nm (~2 μm circular wells) by reactive ion etching, followed by wet etching with buffered hydrofluoric acid etching to remove the SiO_2. The etched SiN_x and SiO_2 acted as a hard mask for subsequent anisotropic Si etching in KOH (33% m/v), following the same procedure as is described elsewhere.[16]

Nanopore devices were cleaned in a 2:1 solution of H_2SO_4/H_2O_2 and subsequently glued using EcoFlex 5 (smooth-on) onto a custom-made Teflon insert, immersed in buffer (1 M KCl, 40 mM Tris-HCl, 1 mM EDTA, pH 7.5), and placed in a Teflon cell. The buffer was filtered using a 0.02 μm syringe filter before use. Two Ag/AgCl pellet electrodes (A-M Systems, Sequim, WA) were connected to an Axon Axopatch 200B patch-clamp amplifier.

Nanopores were drilled in the thinned SiN_x regions using controlled breakdown of dielectric (CBD) as previously reported.[53] An in-house voltage/current amplifier and custom LabVIEW software (National Instruments) were used for the CBD process. Pore formation was terminated when the current exceeded a preset threshold, which was set to ~0.3−0.4 nA measured under 300 mV after each pulse (pulses of 8−9 V with duration of 225 ms). The pore was then expanded using alternating low voltage pulses of 1−3 V with duration of 225 ms to the desired diameter of ~4 nm, estimated according to the open-pore current and the membrane properties (SI Figure S11). The CBD profile was Weibull distributed as previously reported.

Data Acquisition and GMM Analysis. Prior to adding the sample, the nanopores were kept under a low probing voltage (0.15 to 0.3 V) in a buffer solution (1 M KCl, 40 mM Tris-HCl, 1 mM EDTA, pH 7.5) to obtain a stable open-pore current. During the experiment, translocation events were monitored using an Axon 200B amplifier, filtered at 100 kHz, and acquired using a custom LabVIEW software (National Instruments). After collecting the data, we performed offline analysis using a custom LabVIEW program to extract the dwell time (t_D), current blockage (ΔI), and arrival time (t_a) of each translocation event according to an electrical threshold.

SI Figure S4 describes our general data analysis routine. In short, in the first step, density histograms for each axis are generated (x, log-scale of the dwell time; y, blockage amplitude). The peak values of the blockage amplitude and the log-scale dwell time are found, and the mean and covariance matrix (half peak width) is calculated for each peak. The ratio of the peak amplitudes is used as an initial estimate of the mixing proportion. These parameters are used as initial conditions for the GMM algorithm that clusters the data into two groups. The posterior probability, which represents the likelihood that an event belongs to a specified population (GOI and RG), is calculated according to literature[20] and presented as a distribution color map, in which yellow dots correspond to the higher probability (>0.7) of belonging to a specific population. Data analysis was performed using MATLAB (MathWorks, Natick, MA). All graphs and corresponding fits were plotted using Igor Pro 6 (Wavemetrics, Lake Oswego, OR).

ASSOCIATED CONTENT

Supporting Information

The Supporting Information is available free of charge at https://pubs.acs.org/doi/10.1021/acsnano.0c06375.

Schematic illustration and gel validation of MACC1, S100A4, and G6PDH amplicons; ionic current after addition of a "−RT" sample to the nanopore; comparison of DNA translocation events with and without purification; data analysis procedure for separating populations of events based on a Gaussian mixture model (GMM); gel electrophoresis of cDNA fragments prepared from CRC cell lines; calibration curve of MACC1 for the CRC cell lines samples, obtained by RT-qPCR; RT-qNP results for MACC1 cDNA samples after optional PCR amplification; amplification curves for MACC1 obtained by RT-qPCR using hybridization probes; gel electrophoresis of cDNA fragments obtained from SARS-CoV-2 RNA; RT-qNP quantification of SARS-CoV-2 RNA against the human reference gene RPP30 at three concentration ratios; noise spectra and current−voltage (IV) curves of a nanopore; RT-qNP quantification repeats of the SW480 cell line; supplementary tables including gene-specific primers used in nanopore sensing experiments and for validation of cDNA targets by sequencing, gene-specific primers used in RT-qPCR experiments, and gene-specific primers used in SARS-CoV-2 experiments; supplementary notes including sample preparation, optimizing conditions for synthesis and multiplex detection of cDNA targets, negative control of purification-free assay and nanopore sensing,

https://dx.doi.org/10.1021/acsnano.0c06375
ACS Nano 2020, 14, 13964−13974

controls and characteristics of the CRC cell-line sample using multiplex sensing, nanopore fabrication using CBD, and characterization (PDF)

AUTHOR INFORMATION

Corresponding Authors

Ulrike Stein − *Experimental and Clinical Research Center, Charité Universitätsmedizin, Berlin 10117, Germany; Max-Delbrück-Center for Molecular Medicine in the Helmholtz Association, Berlin 13125, Germany; German Cancer Consortium, Heidelberg 69120, Germany*; Email: ustein@mdc-berlin.de

Amit Meller − *Department of Biomedical Engineering, The Technion—IIT, Haifa 32000, Israel;* orcid.org/0000-0001-7082-0985; Email: ameller@technion.ac.il

Authors

Yana Rozevsky − *Department of Biomedical Engineering, The Technion—IIT, Haifa 32000, Israel*

Tal Gilboa − *Department of Biomedical Engineering, The Technion—IIT, Haifa 32000, Israel; Department of Pathology, Brigham and Women's Hospital, Harvard Medical School, Boston, Massachusetts 02115, United States; Wyss Institute, Harvard University, Boston, Massachusetts 02115, United States*

Xander F. van Kooten − *Department of Biomedical Engineering, The Technion—IIT, Haifa 32000, Israel;* orcid.org/0000-0003-2411-6174

Dennis Kobelt − *Experimental and Clinical Research Center, Charité Universitätsmedizin, Berlin 10117, Germany; Max-Delbrück-Center for Molecular Medicine in the Helmholtz Association, Berlin 13125, Germany; German Cancer Consortium, Heidelberg 69120, Germany*

Diana Huttner − *Department of Biomedical Engineering, The Technion—IIT, Haifa 32000, Israel*

Complete contact information is available at: https://pubs.acs.org/10.1021/acsnano.0c06375

Notes

The authors declare no competing financial interest.

ACKNOWLEDGMENTS

We thank Eran Zvuloni and Adam Zrehen for their assistance in nanochip fabrication. We also thank Pia Herrmann, ECRC, Charité—Universitätsmedizin Berlin and Max-Delbrück-Center for Molecular Medicine, Berlin, for technical assistance. This project has received funding from the European Research Council (ERC) under the European Union's Horizon 2020 research and innovation program Grant Agreement No. 833399 and from ISF Award 3485/19. Further, this project was supported by the German−Israel Graduate School SignGene and in part by the German Cancer Consortium (DKTK).

REFERENCES

(1) Pichon, X.; Lagha, M.; Mueller, F.; Bertrand, E. A Growing Toolbox to Image Gene Expression in Single Cells: Sensitive Approaches for Demanding Challenges. *Mol. Cell* **2018**, *71*, 468−480.

(2) Wanunu, M.; Morrison, W.; Rabin, Y.; Grosberg, A. Y.; Meller, A. Electrostatic Focusing of Unlabeled DNA into Nanoscale Pores Using a Salt Gradient. *Nat. Nanotechnol.* **2010**, *5*, 160−165.

(3) Freedman, K. J.; Otto, L. M.; Ivanov, A. P.; Barik, A.; Oh, S.-H.; Edel, J. B. Nanopore Sensing at Ultra-Low Concentrations Using Single-Molecule Dielectrophoretic Trapping. *Nat. Commun.* **2016**, *7*, 10217.

(4) Dekker, C. Solid-State Nanopores. *Nat. Nanotechnol.* **2007**, *2*, 209−215.

(5) Lu, S. M.; Peng, Y. Y.; Ying, Y. L.; Long, Y. T. Electrochemical Sensing at a Confined Space. *Anal. Chem.* **2020**, *92*, 5621−5644.

(6) Wanunu, M.; Sutin, J.; McNally, B.; Chow, A.; Meller, A. DNA Translocation Governed by Interactions with Solid-State Nanopores. *Biophys. J.* **2008**, *95*, 4716−4725.

(7) Keyser, U. F. Enhancing Nanopore Sensing with DNA Nanotechnology. *Nat. Nanotechnol.* **2016**, *11*, 106−108.

(8) Feng, J.; Liu, K.; Bulushev, R. D.; Khlybov, S.; Dumcenco, D.; Kis, A.; Radenovic, A. Identification of Single Nucleotides in MoS_2 Nanopores. *Nat. Nanotechnol.* **2015**, *10*, 1070−1076.

(9) Singer, A.; Rapireddy, S.; Ly, D. H.; Meller, A. Electronic Barcoding of a Viral Gene at the Single-Molecule Level. *Nano Lett.* **2012**, *12*, 1722−1728.

(10) Wanunu, M.; Dadosh, T.; Ray, V.; Jin, J.; McReynolds, L.; Drndić, M. Rapid Electronic Detection of Probe-Specific MicroRNAs Using Thin Nanopore Sensors. *Nat. Nanotechnol.* **2010**, *5*, 807−814.

(11) Wang, Y.; Zheng, D.; Tan, Q.; Wang, M. X.; Gu, L. Q. Nanopore-Based Detection of Circulating MicroRNAs in Lung Cancer Patients. *Nat. Nanotechnol.* **2011**, *6*, 668−674.

(12) Plesa, C.; Kowalczyk, S. W.; Zinsmeester, R.; Grosberg, A. Y.; Rabin, Y.; Dekker, C. Fast Translocation of Proteins through Solid State Nanopores. *Nano Lett.* **2013**, *13*, 658−663.

(13) Nir, I.; Huttner, D.; Meller, A. Direct Sensing and Discrimination among Ubiquitin and Ubiquitin Chains Using Solid-State Nanopores. *Biophys. J.* **2015**, *108*, 2340−2349.

(14) Yusko, E. C.; Johnson, J. M.; Majd, S.; Prangkio, P.; Rollings, R. C.; Li, J.; Yang, J.; Mayer, M. Controlling Protein Translocation through Nanopores with Bio-Inspired Fluid Walls. *Nat. Nanotechnol.* **2011**, *6*, 253−260.

(15) Talaga, D. S.; Li, J. Single-Molecule Protein Unfolding in Solid State Nanopores. *J. Am. Chem. Soc.* **2009**, *131*, 9287−9297.

(16) Squires, A.; Atas, E.; Meller, A. Nanopore Sensing of Individual Transcription Factors Bound to DNA. *Sci. Rep.* **2015**, *5*, 11643.

(17) Singer, A.; Wanunu, M.; Morrison, W.; Kuhn, H.; Frank-Kamenetskii, M.; Meller, A. Nanopore Based Sequence Specific Detection of Duplex DNA for Genomic Profiling. *Nano Lett.* **2010**, *10*, 738−742.

(18) Yang, J.; Wang, Y.; Li, M.; Ying, Y.-L.; Long, Y.-T. Direct Sensing of Single Native RNA with a Single-Biomolecule Interface of Aerolysin Nanopore. *Langmuir* **2018**, *34*, 14940−14945.

(19) Hiratani, M.; Kawano, R. DNA Logic Operation with Nanopore Decoding to Recognize MicroRNA Patterns in Small Cell Lung Cancer. *Anal. Chem.* **2018**, *90*, 8531−8537.

(20) Squires, A. H.; Atas, E.; Meller, A. Genomic Pathogen Typing Using Solid-State Nanopores. *PLoS One* **2015**, *10*, No. e0142944.

(21) VanGuilder, H. D.; Vrana, K. E.; Freeman, W. M. Twenty-Five Years of Quantitative PCR for Gene Expression Analysis. *BioTechniques* **2008**, *44*, 619−626.

(22) Tellinghuisen, J.; Spiess, A. N. Comparing Real-Time Quantitative Polymerase Chain Reaction Analysis Methods for Precision, Linearity, and Accuracy of Estimating Amplification Efficiency. *Anal. Biochem.* **2014**, *449*, 76−82.

(23) Radhakrishnan, H.; Walther, W.; Zincke, F.; Kobelt, D.; Imbastari, F.; Erdem, M.; Kortüm, B.; Dahlmann, M.; Stein, U. MACC1—The First Decade of a Key Metastasis Molecule from Gene Discovery to Clinical Translation. *Cancer Metastasis Rev.* **2018**, *37*, 805−820.

(24) Dahlmann, M.; Kobelt, D.; Walther, W.; Mudduluru, G.; Stein, U. S100A4 in Cancer Metastasis: WNT Signaling-Driven Interventions for Metastasis Restriction. *Cancers* **2016**, *8*, 59.

(25) Stein, U.; Walther, W.; Arlt, F.; Schwabe, H.; Smith, J.; Fichtner, I.; Birchmeier, W.; Schlag, P. M. MACC1, a Newly Identified Key Regulator of HGF-MET Signaling, Predicts Colon Cancer Metastasis. *Nat. Med.* **2009**, *15*, 59−67.

(26) Zhao, Y.; Dai, C.; Wang, M.; Kang, H.; Lin, S.; Yang, P.; Liu, X.; Liu, K.; Xu, P.; Zheng, Y.; Li, S.; Dai, Z. Clinicopathological and Prognostic Significance of Metastasis-Associated in Colon Cancer-1

(MACC1) Overexpression in Colorectal Cancer: A Meta-Analysis. *Oncotarget* **2016**, *7*, 62966−62975.
(27) Link, T.; Kuhlmann, J. D.; Kobelt, D.; Herrmann, P.; Vassileva, Y. D.; Kramer, M.; Frank, K.; Göckenjan, M.; Wimberger, P.; Stein, U. Clinical Relevance of Circulating MACC1 and S100A4 Transcripts for Ovarian Cancer. *Mol. Oncol.* **2019**, *13*, 1268−1279.
(28) Wang, G.; Fu, Z.; Li, D. MACC1 Overexpression and Survival in Solid Tumors: A Meta-Analysis. *Tumor Biol.* **2015**, *36*, 1055−1065.
(29) Hagemann, C.; Neuhaus, N.; Dahlmann, M.; Kessler, A.; Kobelt, D.; Herrmann, P.; Eyrich, M.; Freitag, B.; Linsenmann, T.; Monoranu, C.; Ernestus, R.; Löhr, M.; Stein, U. Circulating MACC1 Transcripts in Glioblastoma Patients Predict Prognosis and Treatment Response. *Cancers* **2019**, *11*, 825.
(30) Stein, U.; Burock, S.; Herrmann, P.; Wendler, I.; Niederstrasser, M.; Wernecke, K. D.; Schlag, P. M. Circulating MACC1 Transcripts in Colorectal Cancer Patient Plasma Predict Metastasis and Prognosis. *PLoS One* **2012**, *7*, e49249−10.
(31) Huang, Y.; Zhang, H.; Cai, J.; Fang, L.; Wu, J.; Ye, C.; Zhu, X.; Li, M. Overexpression of MACC1 and Its Significance in Human Breast Cancer Progression. *Cell Biosci.* **2013**, *3*, 16.
(32) Burock, S.; Herrmann, P.; Wendler, I.; Niederstrasser, M.; Wernecke, K. D.; Stein, U. Circulating Metastasis Associated in Colon Cancer 1 Transcripts in Gastric Cancer Patient Plasma as Diagnostic and Prognostic Biomarker. *World J. Gastroenterol.* **2015**, *21*, 333−341.
(33) Wang, G.; Kang, M. X.; Lu, W. J.; Chen, Y.; Zhang, B.; Wu, Y. L. MACC1: A Potential Molecule Associated with Pancreatic Cancer Metastasis and Chemoresistance. *Oncol. Lett.* **2012**, *4*, 783−791.
(34) Sun, D.-W.; Zhang, Y.-Y.; Qi, Y.; Liu, G.-Q.; Chen, Y.-G.; Ma, J.; Lv, G.-Y. Prognostic and Clinicopathological Significance of MACC1 Expression in Hepatocellular Carcinoma Patients: A Meta-Analysis. *Int. J. Clin. Exp. Med.* **2015**, *8*, 4769−4777.
(35) Liu, Z.; Liu, H.; Pan, H.; Du, Q.; Liang, J. Clinicopathological Significance of S100A4 Expression in Human Hepatocellular Carcinoma. *J. Int. Med. Res.* **2013**, *41*, 457−462.
(36) Huang, S.; Zheng, J.; Huang, Y.; Song, L.; Yin, Y.; Ou, D.; He, S.; Chen, X.; Ouyang, X. Impact of S100A4 Expression on Clinicopathological Characteristics and Prognosis in Pancreatic Cancer: A Meta-Analysis. *Dis. Markers* **2016**, *2016*, 8137378.
(37) Stein, U.; Arlt, F.; Walther, W.; Smith, J.; Waldman, T.; Harris, E. D.; Mertins, S. D.; Heizmann, C. W.; Allard, D.; Birchmeier, W.; Schlag, P. M.; Shoemaker, R. H. The Metastasis-Associated Gene S100A4 Is a Novel Target of β-Catenin/T-Cell Factor Signaling in Colon Cancer. *Gastroenterology* **2006**, *131*, 1486−1500.
(38) Stein, U.; Burock, S.; Herrmann, P.; Wendler, I.; Niederstrasser, M.; Wernecke, K. D.; Schlag, P. M. Diagnostic and Prognostic Value of Metastasis Inducer S100A4 Transcripts in Plasma of Colon, Rectal, and Gastric Cancer Patients. *J. Mol. Diagn.* **2011**, *13*, 189−198.
(39) Liu, W.; Saint, D. A. A New Quantitative Method of Real Time Reverse Transcription Polymerase Chain Reaction Assay Based on Simulation of Polymerase Chain Reaction Kinetics. *Anal. Biochem.* **2002**, *302*, 52−59.
(40) Stein, U.; Jürchott, K.; Schläfke, M.; Hohenberger, P. Expression of Multidrug Resistance Genes MVP, MDR1, and MRP1 Determined Sequentially before, during, and after Hyperthermic Isolated Limb Perfusion of Soft Tissue Sarcoma and Melanoma Patients. *J. Clin. Oncol.* **2002**, *20*, 3282−3292.
(41) Dorak, M. T. Real-Time PCR. *BIOS Advanced Methods*; Taylor & Francis: New York, 2007.
(42) Kainz, P. The PCR Plateau Phase - Towards an Understanding of Its Limitations. *Biochim. Biophys. Acta, Gene Struct. Expression* **2000**, *1494*, 23−27.
(43) Corman, V. M.; Landt, O.; Kaiser, M.; Molenkamp, R.; Meijer, A.; Chu, D. K. W.; Bleicker, T.; Brünink, S.; Schneider, J.; Schmidt, M. L.; Mulders, D. G. J. C.; Haagmans, B. L.; van der Veer, B.; van den Brink, S.; Wijsman, L.; Goderski, G.; Romette, J.-L.; Ellis, J.; Zambon, M.; Peiris, M.; et al. Detection of 2019 Novel Coronavirus (2019-nCoV) by Real-Time RT-PCR. *Euro Surveill.* **2020**, *25*, 2000045.
(44) Chan, J. F.-W.; Yip, C. C.-Y.; To, K. K.-W.; Tang, T. H.-C.; Wong, S. C.-Y.; Leung, K.-H.; Fung, A. Y.-F.; Ng, A. C.-K.; Zou, Z.; Tsoi, H.-W.; Choi, G. K.-Y. C.; Tam, A. R.; Cheng, V. C.-C.; Chan, K.-H.; Tsang, O. T.-Y; Yuen, K.-Y.; et al. Improved Molecular Diagnosis of COVID-19 by the Novel, Highly Sensitive and Specific COVID-19-RdRp/Hel Real-Time Reverse Transcription-PCR Assay Validated *In Vitro* and with Clinical Specimens. *J. Clin. Microbiol.* **2020**, *58*, e00310.
(45) Chu, D. K. W.; Pan, Y.; Cheng, S. M. S.; Hui, K. P. Y.; Krishnan, P.; Liu, Y.; Ng, D. Y. M.; Wan, C. K. C.; Yang, P.; Wang, Q.; Peiris, M.; Poon, L. L. M. Molecular Diagnosis of a Novel Coronavirus (2019-NCoV) Causing an Outbreak of Pneumonia. *Clin. Chem.* **2020**, *66*, 549−555.
(46) He, X.; Lau, E. H. Y.; Wu, P.; Deng, X.; Wang, J.; Hao, X.; Lau, Y. C.; Wong, J. Y.; Guan, Y.; Tan, X.; Mo, X.; Chen, Y.; Liao, B.; Chen, W.; Hu, F.; Zhang, Q.; Zhong, M.; Wu, Y.; Zhao, L.; Zhang, F.; et al. Temporal Dynamics in Viral Shedding and Transmissibility of COVID-19. *Nat. Med.* **2020**, *26*, 672−675.
(47) Heerema, S. J.; Vicarelli, L.; Pud, S.; Schouten, R. N.; Zandbergen, H. W.; Dekker, C. Probing DNA Translocations with Inplane Current Signals in a Graphene Nanoribbon with a Nanopore. *ACS Nano* **2018**, *12*, 2623−2633.
(48) Liu, K.; Feng, J.; Kis, A.; Radenovic, A. Atomically Thin Molybdenum Disulfide Nanopores with High Sensitivity for DNA Translocation. *ACS Nano* **2014**, *8*, 2504−2511.
(49) Traversi, F.; Raillon, C.; Benameur, S. M.; Liu, K.; Khlybov, S.; Tosun, M.; Krasnozhon, D.; Kis, A.; Radenovic, A. Detecting the Translocation of DNA through a Nanopore Using Graphene Nanoribbons. *Nat. Nanotechnol.* **2013**, *8*, 939−945.
(50) Chien, C. C.; Shekar, S.; Niedzwiecki, D. J.; Shepard, K. L.; Drndić, M. Single-Stranded DNA Translocation Recordings through Solid-State Nanopores on Glass Chips at 10 MHz Measurement Bandwidth. *ACS Nano* **2019**, *13*, 10545−10554.
(51) Wang, R.; Gilboa, T.; Song, J.; Huttner, D.; Grinstaff, M. W.; Meller, A. Single-Molecule Discrimination of Labeled DNAs and Polypeptides Using Photoluminescent-Free TiO_2 Nanopores. *ACS Nano* **2018**, *12*, 11648−11656.
(52) Spitzberg, J. D.; van Kooten, X. F.; Bercovici, M.; Meller, A. Microfluidic Device for Coupling Isotachophoretic Sample Focusing with Nanopore Single-Molecule Sensing. *Nanoscale* **2020**, *12*, 17805−17811.
(53) Zrehen, A.; Gilboa, T.; Meller, A. Real-Time Visualization and Sub-Diffraction Limit Localization of Nanometer-Scale Pore Formation by Dielectric Breakdown. *Nanoscale* **2017**, *9*, 16437−16445.

https://dx.doi.org/10.1021/acsnano.0c06375
ACS Nano 2020, 14, 13964−13974